Optical Inspection of Welding Seams

Fabian Timm[1,2], Thomas Martinetz[1], and Erhardt Barth[1,2]

[1] Institute for Neuro- and Bioinformatics, University of Lübeck
Ratzeburger Allee 160, D-23538 Lübeck, Germany
[2] Pattern Recognition Company GmbH
Maria-Goeppert-Strasse 1, D-23562 Lübeck, Germany

Abstract. We present a framework for automatic inspection of welding seams based on specular reflections. To this end, we make use of a feature set – called specularity features (SPECs) – that describes statistical properties of specular reflections. For the classification we use a one-class support-vector approach. We show that the SPECs significantly outperform other approaches since they capture more complex characteristics and dependencies of shape and geometry. We obtain an error rate of 3.8%, which corresponds to the level of human performance.

1 Introduction

In many industrial processes individual parts are joined by using welding techniques. Soldering and welding techniques are common in diverse areas such as printed circuit board assembly or automotive line spot welding. The quality of a single welding often defines the grade of the whole product, for example in critical areas such as automotive or aviation industry, where failures of the welding process can cause a malfunction of the whole product. Typically, welds are made by a laser or a soldering iron. During the last few years lasers and their usage in industrial applications have become affordable for many companies. Although the initial cost of a laser-welding system is still high, their wear-out is low and so the service intervals become very long. A laser weld is more precise than a weld by a soldering iron, but the quality can also vary due to shifts of the part towards the laser or due to material impurities. Therefore, an inspection of the welding is required in order to guarantee an accurate quality.

There are several machine vision approaches to automatically classify the quality of solder joints. These approaches can be divided into two groups. The first group deals with special camera and lighting setups to gain the best image representation of relevant features [1,2,3]. In the second group, the camera and lighting setup is often predetermined and the inspection is done by sophisticated pattern recognition methods. In the last few years several approaches for automatic inspection of solder joints concerning feature extraction, feature selection, and classification have been proposed [4,5,1,6,2]. As in many other applications, neural networks and especially the support-vector-machine have become state-of-the-art [7,8,9].

In this work, we focus on the inspection of cathodes welded by an Nd:YAG (neodymium-doped yttrium aluminium garnet) laser during the production of lamps. Due to its position in the whole production process, the camera and lighting setup was fixed and could not be changed.

A. Ranchordas et al. (Eds.): VISIGRAPP 2009, CCIS 68, pp. 269–282, 2010.

Since the welded cathode has specific specular reflections, an appropriate feature extraction is required in order to achieve an accurate performance. Therefore, we apply a feature set called specularity features (SPECs) [10]. The SPECs contain statistics of certain shape characteristics of single components and can cover a wide range of complex shape properties and their dependencies. Since only the class of accurate weldings is sampled properly, we use a one-class support-vector approach [11,12,13] in order to describe features of accurate weldings and to separate them from all other possible inaccurate weldings. We also evaluate those SPECs that are most relevant for the classification and compare them to the physical shape of the cathode. For comparison we use raw pixel intensities, radial encoded raw pixel intensities and the statistical geometric feature (SGF) algorithm that computes simple geometric characteristics of binary components.

In section 2 we give a brief overview of the camera and lighting setting and the image acquisition. The methods for feature extraction and classification are described in section 3. Experiments and the results are shown in section 4. We conclude with a discussion in section 5.

2 Image Acquisition

An unwelded cathode consists of a socket and a pole that may be composed of different materials (see Fig. 1). In a top view with directional parallel light the unwelded cathode simplifies to only four components – two black rings (the slant of the neck and the space between pin and socket), one white ring (neck of the socket) and one white circle (top of the pin, see Fig. 1 bottom right). Hence, a component analysis of the grey value image of the welded cathode can be used to extract specific features.

A correct combination of camera, lens and illumination is very important to achieve the best performance in classification. However, sometimes the best setup can not be chosen due to limited space or other requirements. For this work, there was only one camera setup practicable (see Fig. 2). We used a standard analog monochrome VGA video camera, a single-sided telecentric lens and an LED ring light with a Fresnel lens. Each image contained a single cathode that we extracted by applying a hough-transformation. We removed images of unwelded cathodes and images that are classified easily from the dataset to reduce the amount of images. Thus, the dataset consisted only of images of welded cathodes that are difficult to classify manually. In total, we collected 934 images containing 657 images of non-defective cathodes and 277 images of defective cathodes.

Each image was labelled by experts, scaled to different sizes (10×10, 20×20, 40×40, 80×80 px) and smoothed by a Gaussian filter ($\sigma = 1$). Since we also use raw pixel intensities, we rotated each image four times ($0, \frac{1}{2}\pi, \pi, \frac{3}{2}\pi$) giving a total amount of 3736 images. Since defective cathodes are determined by the mean time to failure, the true class labels are not known in general. Therefore, the experts look for aberrations that were selected by extensive benchmark tests. Example images of defective and non-defective cathodes are shown in Fig. 3. The reflections of cathodes without a defect vary due to differences in material and position of the pin. Also, a slight deflection of the pin just before the welding can affect the quality of the welding. Some of the defective cathodes have holes caused by a slanted pin, others do not have any reflections

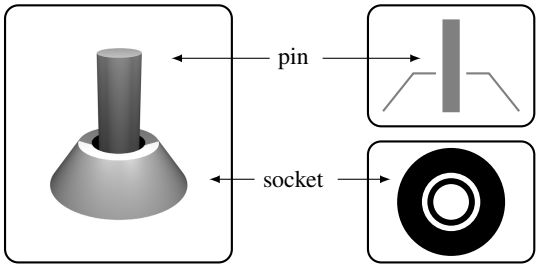

Fig. 1. A 3D drawing of the cathode (left), a cross-section (upper right) and a top-view image are shown (lower right)

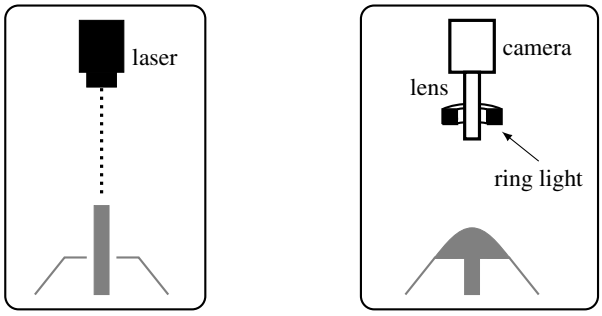

Fig. 2. Drawing of the setup for laser welding (left) and image acquisition (right). The laser and the camera are located on top of the cathode.A Fresnel lens was mounted in front of the ring light to obtain bright illumination at the cathode.

due to a very rough surface. Therefore, the variety of defects cannot be described easily, and a feature extraction method that covers specific image properties such as properties based on specular reflections is required.

3 Methods

Recently, several approaches for the inspection of solder joints were proposed [1,3,4,2,6]. Some of these methods compute simple features in a manually tiled binary image, others use the pixel intensities directly as input features for a neural network or a support vector machine [7,8,9]. Since the number of pixels is very large compared to the number

Fig. 3. Example images of defect-free (left) and defective cathodes (right)

of data samples, the preprocessing often involves a downsampling of the images in order to reduce the dimensionality considerably. Usually, this downsampling reduces the information contained in the images significantly and therefore yields poor error rates. A better performance is achieved by extracting specific features that describe relevant image properties, e.g. specularity features for the case of welding seam inspection.

In the following, we will describe the extraction of SGFs and SPECs. Since the images were recorded by an 8bit monochrome camera, we focus on grey value images, but the approach can easily be extended to colour images.

3.1 Statistical Geometric Features

Originally, SGFs were used for texture classification with 16 features for each image [14]. Further extensions were developed for cell nuclei classification and contained 48 features [15]. SGFs compute simple shape properties of local components. Hence, they can be used to extract specific features of welding images. Moreover, SGFs are very intuitive and computed efficiently.

For each l-bit grey value image I a stack of binary images $\mathcal{B} = \{I_\tau\}$ with $\tau \in \{1, 2, 3, ..., 2^l\}$ is created. A single binary image I_τ is computed such that

$$I_\tau(x, y) = \begin{cases} 1 & : \quad I(x, y) \geq \tau \\ 0 & : \quad I(x, y) < \tau \end{cases} \quad . \tag{1}$$

This decomposition is lossless, since the input image can always be recovered by summing up all binary images. Furthermore, each binary image I_τ is decomposed into a set of black and white components, $\{\mathbf{C}_0(\tau), \mathbf{C}_1(\tau)\}$ with $\mathbf{C}_0(\tau) = \{C_{(0,\tau)_1}, ..., C_{(0,\tau)_m}\}$ and $\mathbf{C}_1(\tau) = \{C_{(1,\tau)_1}, ..., C_{(1,\tau)_n}\}$, where m and n are the numbers of black and white components (see Fig. 4). In the following the subscript 0 denotes a black component and the subscript 1 a white component.

Each component $C_{(j,\tau)_i} = \{\boldsymbol{x}_k\}$ consists of pixel positions $\boldsymbol{x}_k \in \{1, 2, ..., H\} \times \{1, 2, ..., W\}$, where H and W are the height and the width of the input image, respectively. For convenience we omit the indices of a component if they are not necessary and we use $C_i = C_{(j,\tau)_i}$ for abbreviation.

The area of a component is defined by the number of its pixels and the relative size of a single component C_i with respect to all components is then defined as

$$\texttt{PROP}\,(C_i) = \frac{\texttt{AREA}\,(C_i)}{\sum_k \texttt{AREA}\,(C_k)} \quad . \tag{2}$$

Based on the stack of binary images, the feature extraction of the SGF algorithm can be divided into two stages – a local stage and a global stage. In the local stage several features for each component are calculated (see Tab. 1). A single binary image is then described by a set of averaged shape and position properties of all black and white components.

In the second stage the local features are combined to global features using first order statistics (see Tab. 2). In total, the SGF algorithm determines 48 shape properties for a single input image.

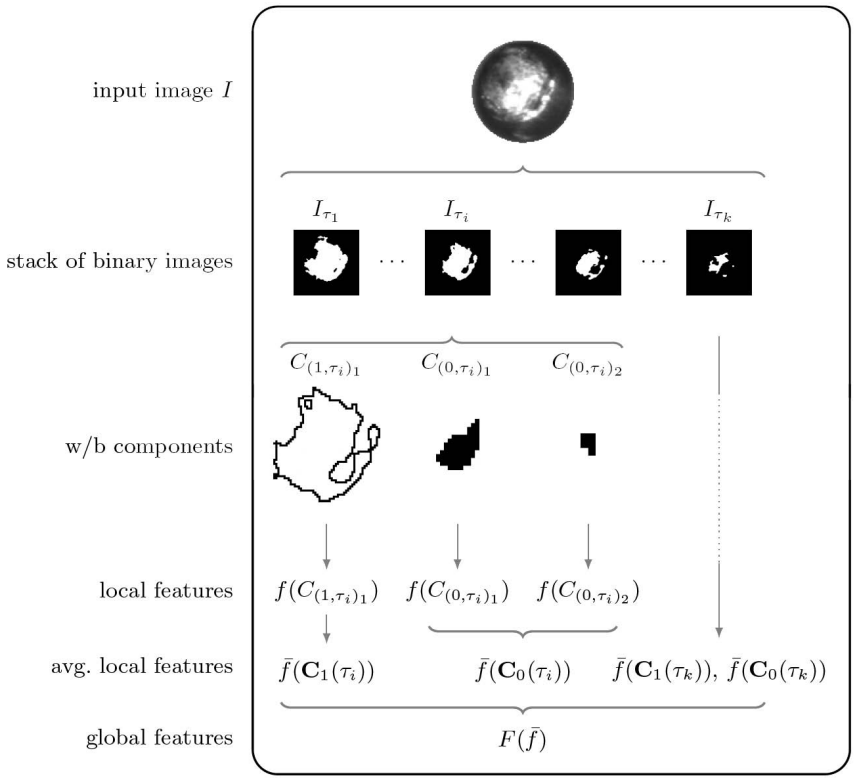

Fig. 4. Decomposition scheme for a grey value input image I. First, the input image is decomposed into a stack of binary images I_τ. Afterwards each binary image is further separated into its black and white components. Local features f, e.g. the area, are computed for all components and averaged according to their component colour. Finally, global features F are generated by computing statistics over all averaged local features.

3.2 Specularity Features (SPEC)

Since the statistical geometric features were mainly developed for classification of textures, i.e. repetitive patterns, they are not suitable for the inspection of welding seams, which usually do not have a repetitive structure. Instead, properties that describe the characteristic shapes of specular reflections are required. For example, some defective cathodes have long narrow reflections at the neck of the socket which can be covered by features such as the formfactor and the extent.

We make use of the general decomposition scheme of binary images and evaluate appropriate features covering the properties of specular reflections. We compute several general properties of each component (see Tab. 3). Using a 4-neighbourhood two successive boundary points are denoted by $\boldsymbol{x}_m$ and $\boldsymbol{x}_{m+1}$, $F(\alpha)$ is the maximum distance between two boundary points when rotating the coordinate axis by $\alpha \in \mathcal{A} = \{0°, 5°, ..., 175°\}$, w_{BR} and h_{BR} are the width and height of the bounding rectangle and a, b are the major and minor axis of the ellipse that has the same second moments as the region. For a detailed discussion on geometric shapes see chapter 9 of [16].

Table 1. Local features for a single binary image I_τ of size $H \times W$ [15]

description	formula		
number of b/w components	$\texttt{NOC}(\tau)$	$=$	$\lvert\mathbf{C}_i(\tau)\rvert$
averaged irregularity	$\overline{\texttt{IRGL}}\,(\tau)$	$=$	$\frac{\sum_k \texttt{IRGL}(C_k)\ \texttt{AREA}(C_k)}{\sum_k \texttt{AREA}(C_k)}$
averaged clump displacement	$\overline{\texttt{DISP}}(\tau)$	$=$	$\frac{1}{\texttt{NOC}(\tau)} \sum_k \texttt{DISP}(C_k)$
averaged clump inertia	$\overline{\texttt{INERTIA}}(\tau)$	$=$	$\frac{1}{\texttt{NOC}(\tau)} \sum_k \texttt{DISP}(C_k)\,\texttt{AREA}(C_k)$
total clump area	$\texttt{TAREA}(\tau)$	$=$	$\frac{1}{H\,W} \sum_k \texttt{AREA}(C_k)$
averaged clump area	$\overline{\texttt{CAREA}}_i(\tau)$	$=$	$\frac{1}{\texttt{NOC}(\tau)} \sum_k \texttt{AREA}(C_k)$

where

$\texttt{IRGL}\,(C) = \dfrac{1 + \sqrt{\pi}\ \max_{\boldsymbol{x} \in C}\ \|\boldsymbol{x} - \mu(C)\|}{\sqrt{\texttt{AREA}(C)}} - 1$ is the irregularity of component C,

$\texttt{DISP}(C) = \sqrt{\pi}\ \dfrac{\|\mu(C) - \mu_I\|}{\sqrt{H\,W}}$ is the relative displacement of component C,

$\mu(C)$ is the centre of gravity of component C and μ_I is the centre of the image.

Table 2. Global features. f is one of the local features described before.

$\texttt{maximum}$	$= \max_\tau f(\tau)$	, $\texttt{mean}$	$= \frac{1}{\lvert\tau\rvert} \sum_\tau f(\tau)$
$\texttt{sample mean}$	$= \frac{1}{\sum_\tau f(\tau)} \sum_\tau \tau\, f(\tau)$	, $\texttt{sample std.}$	$= \sqrt{\frac{\sum_\tau (\tau - \texttt{sample mean})^2\, f(\tau)}{\sum_\tau f(\tau)}}$

The local features are computed for each component and need to be combined to form a single feature. Hence, we scale each feature in two different ways. First, we calculate the mean weighted by the relative size of the components, and second, we scale the sum by the total number of components. For example, for the averaged perimeter of the binary image I_τ these two scalings are:

$$\overline{\texttt{PERIM}}(\tau) = \sum_k \texttt{PERIM}(C_k)\ \texttt{PROP}(C_k) \quad \text{and} \quad \overline{\texttt{PERIM}}(\tau) = \frac{1}{\texttt{NOC}(\tau)} \sum_k \texttt{PERIM}(C_k)\ , \tag{3}$$

where $\texttt{PROP}(C_k)$ is defined in Eq. 2. By using these two scalings we can evaluate whether the size of a component is relevant for the feature extraction.

We combine the local features by computing `minimum`, `variance`, `median`, and `entropy` besides the statistics of Tab. 2. Whereas the `sample mean` and `sample std.` range over the threshold τ, the others compute statistics over local shape features. Hence, we can, for example, evaluate the variance of the number of white components or the entropy of the formfactor of white components. In total, for a single image, we determine 448 features consisting of:

- 28 local features for a single component (14 for a black component and 14 for a white component),

Table 3. Features for a component C

feature	formula
perimeter (PERIM)	$\sum_{m=1}^{N-1} \|\boldsymbol{x}_m - \boldsymbol{x}_{m+1}\|_2$
distance from centre (DISTC)	$\|\mu(C) - \mu_I\|_2$
maximum Feret diameter (MAXFD)	$\max_{\alpha \in \mathcal{A}} F(\alpha)$
minimum Feret diameter (MINFD)	$\min_{\alpha \in \mathcal{A}} F(\alpha)$
mean Feret diameter (MEANF)	$\frac{1}{\lvert\mathcal{A}\rvert} \sum_{\alpha \in \mathcal{A}} F(\alpha)$
variance Feret diameter (VARF)	$\frac{1}{\lvert\mathcal{A}\rvert} \sum_{\alpha \in \mathcal{A}} \left[F(\alpha) - \texttt{MEANF}\right]^2$
area of bounding rectangle (AREAB)	$w_{\texttt{BR}}\, h_{\texttt{BR}}$
eccentricity (ECCEN)	$\frac{\sqrt{a^2+b^2}}{a}$
aspect ratio (ASPAR)	$\frac{\texttt{MAXFD}(\tau)}{\texttt{MINFD}(\tau)}$
extent (EXTEN)	$\frac{\texttt{AREA}}{\texttt{AREAB}}$
formfactor (FORMF)	$\frac{4\,\pi\,\texttt{AREA}}{\texttt{PERIM}^2}$
roundness (ROUND)	$\frac{4\,\texttt{AREA}}{\pi\,\texttt{MAXFD}^2}$
compactness (COMPT)	$\frac{2\,\sqrt{\texttt{AREA}}}{\sqrt{\pi}\;\texttt{MAXFD}}$
regularity of aspect ratio (REGAR)	$\left[1 + \texttt{VARFD} + \texttt{MAXFD} - \texttt{MINFD}\right]^{-1}$

- 2 scaling methods (by the proportional size and by the total number of components) and
- 8 global statistics.

3.3 Radial Encoding

The two approaches mentioned in the previous sections are based on image properties. Alternatively, one could use pixel values as input features. This can be further extended by a radial encoding of pixel values (see Fig. 5). Therefore, we divide the input image into several sectors using 8 angles and 6 radii all sampled equally. For each sector we compute the mean intensity to obtain 48 features for an input image, which reflects the fact that we deal with objects in the image that have a circular outline.

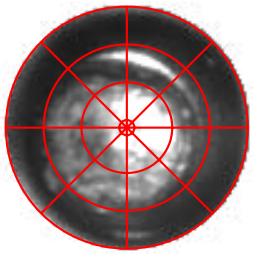

Fig. 5. Radial encoding of an image

3.4 Feature Analysis

Most of the techniques we use for feature extraction generate high-dimensional data. By analysing these feature vectors we want to address two aspects. First, we want to detect features that contain almost no information and remove those features in order to save memory and computation time. Second, we want to evaluate those raw features, SGFs and SPECs that are most discriminative of describing defect-free and defective weldings. Therefore, we use two different approaches, principle component analysis (PCA) and linear discriminant analysis (LDA). For the PCA we take only defect-free samples and evaluate those principle components that have the largest absolute eigenvalues. Although the class of defective weldings is not sampled properly, we also compute the LDA and sort the entries of the resulting weight vector according to their absolute value.

3.5 Classification

The support vector machine (SVM) has become a very useful approach for classification and yields superior performance on several benchmark datasets [7,8,9]. Standard two-class SVMs require samples that describe *both* classes in a proper way. In our case, however, there are only a few defective cathodes that are characterised well. We therefore apply a one-class support-vector machine. Furthermore, we make use of a simple incremental training algorithm with several improvements for fast parameter validation [13,17,12,11]. In contrast to standard two-class SVMs, which separate the input space into two half-spaces, one-class SVMs learn a subspace such as to enclose the samples of only the target class. This increases the robustness against unknown classes of outliers and also extends the time intervals for retraining when new samples are available.

4 Experiments and Results

In the following, we analyse different feature sets with respect to their relevance and we compare them with respect to their classification performance. These feature sets are raw pixel intensities, radially encoded raw pixel intensities, SGFs, and SPECs.

Since the performance of the SGFs can vary depending on the grey level depth of the images we used different depths ranging from 2bit to 8bit [15]. The raw pixel intensities are only used as a baseline.

For the SVM we chose a Gaussian kernel and evaluated the best parameters by 10-fold cross validation. We further scaled the input features to zero mean, unit variance, and unit mean norm and we removed each constant feature to speed up the algorithm and to save memory. For a comparison of the different feature extraction methods we applied a Wilcoxon signed rank test to the test errors.

Since no benchmark datasets of solder joint images are available, we only applied the feature extraction methods to images of laser-weldings.

4.1 Results of Feature Analysis

We analysed the raw pixel intensities using PCA as described in section 3.4. The resulting eigenimages show three important aspects (see Fig. 6).

First, pixels in the centre are more important than pixels at the border of the pole (see Fig. 6, row 2, column 3). This corresponds to the description in Sec. 2 where white reflections (regions) in the centre of the image indicate defect-free weldings. Second, the ring structure, i.e. the area at the neck of the socket, also shows high relevance (see Fig. 6, row 1, column 1). Third, more complex geometric shapes are significant (see Fig. 6, r:1, c:4, r:2, c:1-2). Therefore, a sophisticated feature extraction approach is required in order to describe these complex geometric areas. For describing these areas appropriately than just taking the pixel values we used the radial encoding mentioned in Sec. 3.3. Some of the most significant SGFs are

- the sample std. of irregularity of white components,
- the mean of irregularity of white components,
- the sample std. of total clump area of white components, and
- the mean of displacements of white components.

We analysed the discriminating performance of the SGFs and the SPECs using the LDA as described previously. Therefore, we ranked the features according to their absolute value.

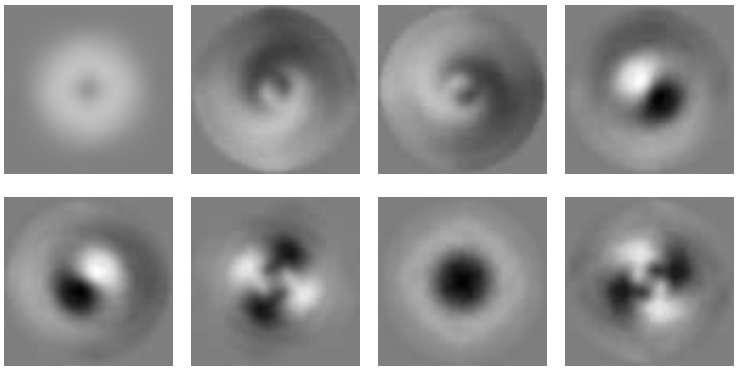

Fig. 6. Eigenimages and eigenvalues using images of size 80×80 and 8 bit grey level depth. Large values (black/white) indicate relevant pixels.

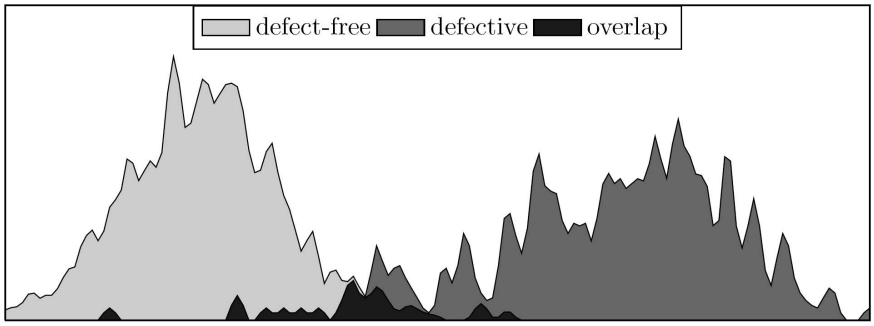

Fig. 7. Class distributions when projecting the SGF features onto the direction obtained by LDA

(a) median of regularity of aspect ratio weighted by area (black components)

(b) median of variance of Feret weighted by NOC (black components)

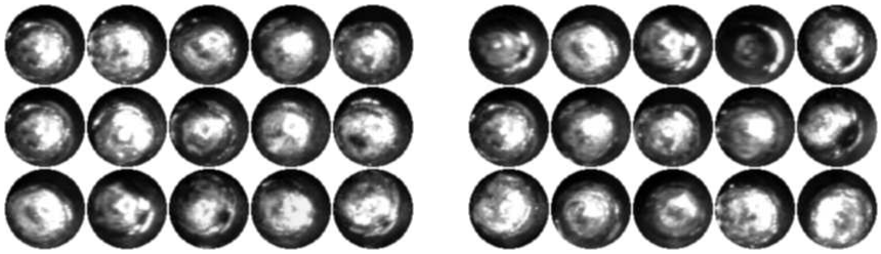

(c) variance of distances from centre weighted by NOC (white components)

(d) sample std. of area of bounding rectangle weighted by NOC (black comp.)

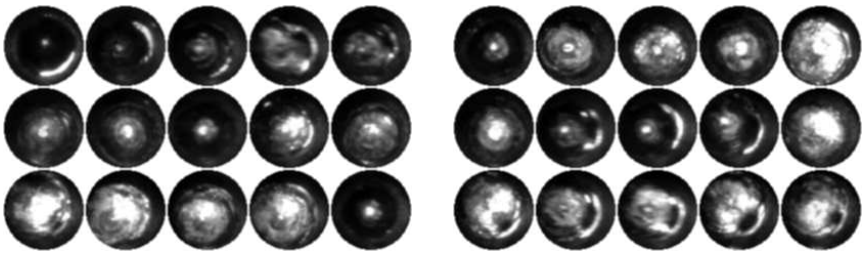

Fig. 8. Example images with large values of the indicated features (top row), medium values (middle row) and small values(bottom row).

This shows that features of white components are more important than those of black components. Further, the shape of components, their positions and their size are relevant properties for the discrimination. If we project the SGFs onto the direction obtained by LDA both classes overlap (see Fig. 7). Thus, in the feature space of SGFs there exists no hyperplane that can separate both classes without making any errors.

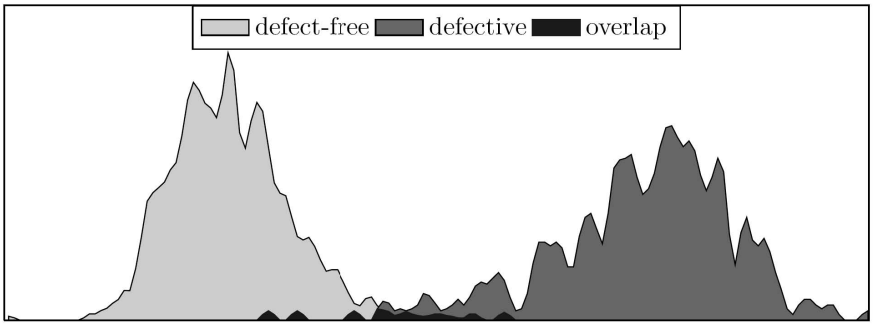

Fig. 9. Class distributions when projecting the SPEC features onto the direction obtained by LDA

Some of the most important SPECs when using the LDA are

- median of regularity of aspect ratio of black components weighted by area (see Fig. 8(a)),
- median of variance of Feret diameter of black components weighted by the number of components (see Fig. 8(b)),
- variance of distances from centre of white components weighted by the number of components (see Fig. 8(c)), and
- sample std. of area of bounding rectangle of black components weighted by the number of black components (see Fig. 8(d)).

This indicates that black components become important when using local features such as the Feret diameter or the bounding rectangle. Since the SGFs are limited to only a few local features, the black components are ignored. Moreover, the area of a component is also relevant as it is used for the scaling of the local features. This becomes more apparent by analysing the ranking of the 100 most relevant SPECs. There, 45 local features are scaled by their area and 55 are scaled by the number of components. Further, 43 local features correspond to black components and 57 correspond to white components. This demonstrates that the properties of the specular reflections cannot be described properly by using raw pixel intensities.

If we project the data onto the LDA direction as we did for the SGFs, the overlap becomes smaller, which indicates that the discrimination power of the SPECs is higher than that of the SGFs (see Fig. 9). However, there also exists no hyperplane separating both classes without an error.

4.2 Results of Classification

The classification results for the different feature extraction approaches to cover complex properties of specular reflections show several aspects.

The radially encoded raw pixel intensities perform significantly better than using raw pixels without any encoding (see Fig. 10). This does not depend on the image size nor on the grey level depth. The best performance of radially encoded raw pixels is obtained using images of size 40×40 pixels and 16 grey levels (error of 13.5%).

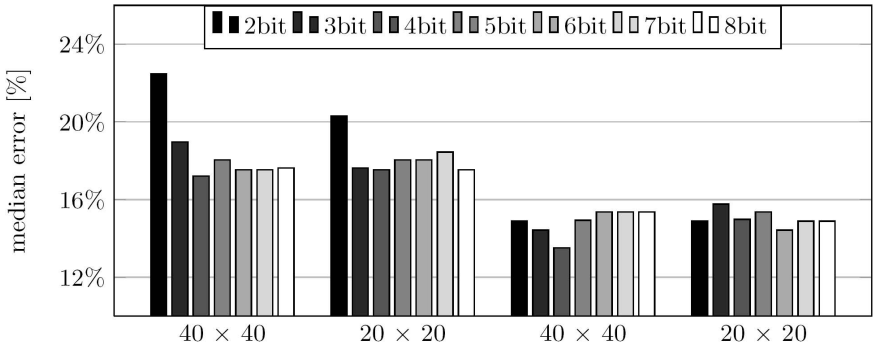

Fig. 10. Classification results using raw pixel intensities and radially encoded pixel intensities for different image sizes and different grey level depths

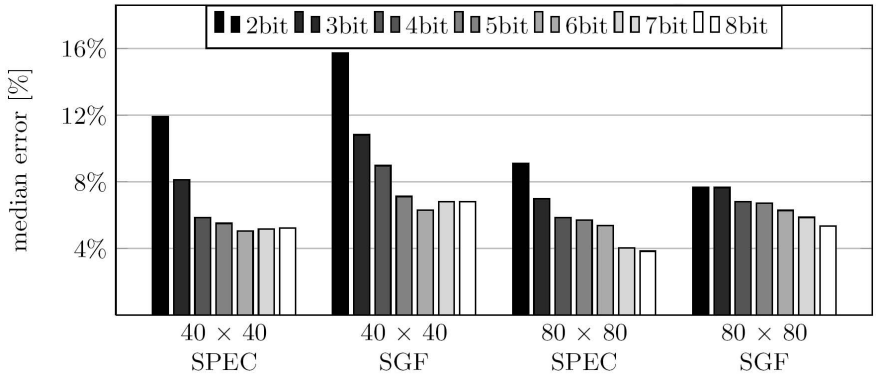

Fig. 11. Classification results using SGFs and SPECs for different image sizes and different grey level depths

Compared to the radial encoding, the SGFs as well as the SPECs improve the classification performance considerably (see Fig. 11). The best performance of the SGFs is achieved by using images of size 80×80 pixels and 256 grey levels with an error of 5.3%. For the same image size and the same number of grey levels the SPECs significantly outperforms ($p = 0.03$) the SGFs with an error of 3.8%. This improvement demonstrates that the SPECs can describe properties of specular reflections more properly than SGFs and radial encoded raw pixels. It further shows that a large number of grey levels is required to describe specular reflections in both cases, for SGFs as well as for the SPECs.

Further, no significant difference between the image sizes could be observed neither for the raw pixel intensities nor for the SGFs and the SPECs, i.e. grey level resolution is more important than spatial resolution (see Fig. 10 and Fig. 11). If the image size is smaller than 10×10 pixels, however, the higher relevance of the grey level depth compared to the image size does not hold, since the structures of the welded pin and the socket are merged, e.g. holes and rings cannot be detected any more.

5 Conclusions

We introduced an approach for the inspection of welding seams using specularity features (SPECs) and showed that these features significantly outperform statistical geometric features as well as raw pixel intensities with and without encoding. We extracted the relevant features of the SPECs and found white regions in the centre of the image and their shape to be of high importance for the classification. The SPECs can cover several complex shape properties and their dependencies and are, nevertheless, intuitive and computed efficiently. Hence, they are well appropriate for the automatic inspection of welding seams and can even be applied to a wider range of machine vision problems concerning complex specular reflections, such as surface inspection or defect detection of specular objects.

The labelling of the datasets of solder joints or other weldings is usually based on experts viewing images and not on the actual functional test. Hence, these labels are very subjective and do not necessarily correspond to the physical and electrical properties of the weldings. Therefore, additional information about the welding, e.g. the conductivity, rigidity, or weld strength, has to be collected and combined with a machine-vision based approach in order to improve the results.

The results may further be improved using other feature selection methods. However, the error rate (3.5%) of the SPEC features are comparable to those obtained by manual inspection.

Acknowledgements. Our research is supported by Philips Technologie GmbH, Global Technology Development Aachen, Germany. Special thanks to Christian Arlt for providing the images and further material.

References

1. Ong, T., Samad, Z., Ratnam, M.: Solder joint inspection with multi-angle imaging and an artificial neural network. The Int. Journal of Advanced Manufacturing Technology 38, 455–462 (2008)
2. Kim, J., Cho, H.: Neural network-based inspection of solder joints using a circular illumination. Image and Vision Computing 13, 479–490 (1995)
3. Chiu, S., Perng, M.: Reflection-area-based feature descriptor for solder joint inspection. Machine Vision and Applications 18, 95–106 (2007)
4. Ko, K., Cho, H.: Solder joints inspection using a neural network and fuzzy rule-based classification method. IEEE Transactions on Electronics Packaging Manufacturing 23, 93–103 (2000)
5. Poechmueller, W., Glesner, M., Listl, L., Mengel, P.: Automatic classification of solder joint images. In: Proc. of the Int. Joint Conf. on Neural Networks, vol. 2, pp. 933–940. IEEE Computer Society Press, Los Alamitos (1991)
6. Driels, M., Lee, C.: Feature selection for automatic visual inspection of solder joints. The Int. Journal of Advanced Manufacturing Technology 3, 3–32 (1988)
7. Cortes, C., Vapnik, V.: Support-vector networks. Machine Learning 20, 273–297 (1995)
8. Boser, B., Guyon, I., Vapnik, V.: A training algorithm for optimal margin classifiers. In: Haussler, D. (ed.) Proc. of the 5th Annual ACM Workshop on Computational Learning Theory, pp. 144–152. ACM Press, New York (1992)

9. Vapnik, V.: The Nature of Statistical Learning Theory. Springer, New York (1995)
10. Timm, F., Klement, S., Martinetz, T., Barth, E.: Welding inspection using novel specularity features and a one-class svm. In: Proc. of the Int. Conference on Imaging Theory and Applications, vol. 1, pp. 146–153. INSTICC (2009)
11. Schölkopf, B., Platt, J.C., Shawe-Taylor, J., Smola, A.J., Williamson, R.C.: Estimating the support of a high-dimensional distribution. Neural Computation 13, 1443–1471 (2001)
12. Tax, D.M.J., Duin, R.P.W.: Support vector data description. Machine Learning 54, 45–66 (2004)
13. Labusch, K., Timm, F., Martinetz, T.: Simple incremental one-class support vector classification. In: Rigoll, G. (ed.) DAGM 2008. LNCS, vol. 5096, pp. 21–30. Springer, Heidelberg (2008)
14. Chen, Y.Q., Nixon, M.S., Thomas, D.W.: Statistical geometrical features for texture classification. Pattern Recognition 28, 537–552 (1995)
15. Walker, R., Jackway, P.T.: Statistical geometric features: Extensions for cytological texture analysis. In: Proc. of the 13th Int. Conf. on Pattern Recognition, pp. 790–794. IEEE Computer Society Press, Los Alamitos (1996)
16. Russ, J.C.: The Image Processing Handbook. CRC Press, Boca Raton (2007)
17. Timm, F., Klement, S., Martinetz, T.: Fast model selection for maxminover-based training of support vector machines. In: Proc. of the 19th Int. Conf. on Pattern Recognition, Florida, USA. IEEE Computer Society Press, Los Alamitos (2008)